SSRG International Journal of Electrical and Electronics Engineering
ISSN: 2348-8379/ https://doi.org/10.14445/23488379/IJEEE-V13I5P101

Volume 13 Issue 5, 1-10, May 2026

Original Article

Design of Reduced-Order Observer-Based Optimal Controller for SMIB System to Enhance Dynamic Stability

K Himaja[1], Venkatampalli Maheswari [2], Sapvath Vinod Kumar[3]

[1,2,3]*Department of Technical Education, Govt Polytechnic, EEE Department, Telangana, India.*

[1]*Corresponding Author : himajak2000@yahoo.co.in*

Received: 04 February 2026 Revised: 03 March 2026 Accepted: 02 April 2026 Published: 30 May 2026

Abstract *- This paper introduces a Reduced-Order Observer–Based Optimal Controller (ROOBC) strategy integrated for a Thyristor-Controlled Series Compensator (TCSC) to effectively enhance the dynamic stability of a unique system. The proposed control scheme employs an ROOBC to estimate the unmeasured system states, like rotor angle, thereby lowering computational complexity while maintaining effective control performance. An Optimal State-Feedback Control (OSFC) law is designed based on the estimated states to improve the system dynamic response under disturbance. The effectiveness of the proposed ROOBC-based TCSC controller is checked on a unique system and compared with conventional TCSC control, Power System Stabilizer (PSS), and the system without control. Stability assessment is carried out through eigenvalue analysis and time-domain simulations at the nominal operating condition. The results demonstrate that the proposed ROOBC-based TCSC significantly enhances dynamic stability and provides superior dynamic performance compared to the other control strategies considered.*

Keywords *- Damping Ratio, Dynamic Stability, Eigenvalues, PSS, ROOBC, TCSC.*

1. Introduction

Electrical Power Systems (EPS), which are complex and inherently nonlinear in nature, are frequently subject to Low-Frequency Oscillations (LFOs) due to their large-scale structure and dynamic behavior. Inter-area and local mode power system oscillations generally occur within a frequency band spanning 0.2 Hz to 2 Hz, and their presence can seriously compromise the dynamic stability of electrical transmission networks [1]. When adequate damping mechanisms are absent, these oscillations tend to grow in magnitude and can ultimately lead to a complete loss of synchronism among generators. While PSS are conventionally employed to mitigate such LFOs, their effectiveness diminishes under conditions of heavy power transfer and long transmission distances, often resulting in sluggish response times. In response to these shortcomings, FACTS-based damping controllers have emerged as a widely utilized solution, providing fast attenuation of oscillations and significantly improving the dynamic stability characteristics of power systems [2-7].

Among the series compensation in the FACTS devices, the TCSC stands out as a pioneering first-generation controller, well-regarded for its dual capability of resolving transient stability challenges and suppressing LFOs, while also being a cost-effective solution [8-9].

Many researchers have recently focused on the impact of TCSC on the stability of Electrical Power Systems (EPS) [10-12]. In [10], a control approach based on the speed difference between generators located at the two ends of a transmission line was used to regulate the TCSC reactance, and the influence of line loading and load characteristics on damping performance was studied through eigenvalue analysis. The authors of [11] proposed a state-feedback control scheme for TCSC using the pole placement technique, in which a suitably designed feedback gain matrix was employed to relocate the closed-loop poles to desired locations, though this approach necessitated the measurement of all system states. More recently, Chang and Chow [12] proposed a time-optimal control scheme for the TCSC, in which a time-based performance index was minimized to achieve fast system response.

At some operating point, the linearized PI controller provides optimal performance. However, when operating conditions change or EPS parameters vary, the fixed structure of conventional damping controllers results in reduced or suboptimal performance [13].

Adaptive controllers are used to handle variations in system parameters and can improve system performance under changing conditions [14]. However, they require online

parameter identification, state observation, and fast gain computation, which restricts their application to low-order systems and limits optimal performance. Various AI-based controllers, including fuzzy logic and FOPID, have been integrated into power networks to mitigate LFOs. However, their performance tends to degrade considerably under significant parameter uncertainties and abrupt load disturbances, which constitutes a notable limitation of these approaches [15]. The dynamic behavior of EPS is governed by fluctuations in system variables, which play a crucial role in the design of effective control strategies. However, obtaining all necessary state variables is not always straightforward, as some may be difficult, impractical, or financially burdensome to measure directly. Given that the deployment of sensors introduces additional costs and renders the system vulnerable to noise and external disturbances, modern control systems increasingly rely on observers as a more practical and reliable alternative for accurately estimating those states that cannot be directly measured [16].

To address the drawbacks inherent in adaptive controllers, intelligent controllers, and physical sensors, a ROOBC is presented as an effective alternative. The proposed approach is characterized by its uncomplicated design and ease of implementation, while maintaining consistent and dependable dynamic performance under varying load conditions and system parameter uncertainties. The ROOBC reconstructs only the necessary system states, thereby reducing computational overhead while effectively preserving the dynamic stability of the system [17-20]. The mathematical model of the ROOBC is presented along with SMIB with TCSC. The paper is structured as follows:

- The mathematical model of SMIB is presented.
- The test system is analyzed through eigenvalues with PSS, TCSC, and ROOBC connected to the test system.
- The controllers are checked on a SMIB test system at nominal load through time response analysis.

2. System Investigated

Figure 1 presents the single generator connected to an infinite transmission line having a line resistance of R_e and reactance X_e. The generator is modeled, incorporating the IEEE Type-1 excitation system along with the decay model. The data of Figure 1 are presented in [21, 22].

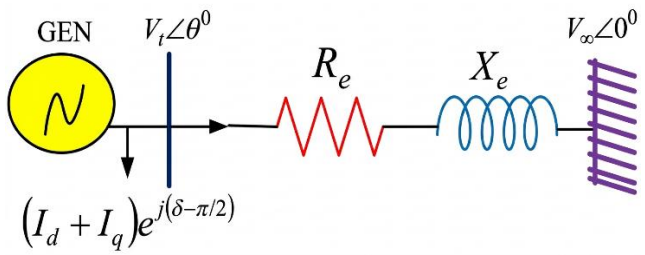

Fig. 1 Single line diagram of a test system

2.1. Evaluation of K Constants

From the steady state equations, calculate the different variables presented in the K- constants of the HP model. These equations and K -constants of the HP model for the test system are presented in [22].

$E = 1.2758 + 1.0637i = 1.6611\angle 0.6950$; $T_M = 0.4155$; $V_{ref} = 1.1762$; $I_d = 0.3437$; $I_q = 0.2051$; $V_d = 0.4115$; $V_q = 1.0974$;$K_1 = 0.7887$; $K_2 = 0.6343$;$K_3 = 0.3938$; $K_4 = 0.9757$; $K_5 = 0.038$ and $K_6 = 0.6988$

The dynamic behavior of the test system is described through the following set of DAE [21].

$$\dot{X} = f(X, Y) \quad (1)$$

$$0 = g(X, Y) \quad (2)$$

Equation (1) captures the differential equations that describe the dynamic behavior of the load, generator, and other associated system components, while the corresponding algebraic constraints are expressed through Equation (2).

In order to assess the dynamic stability of the system via eigenvalue analysis, both sets of equations are linearized in the vicinity of a nominal operating point, resulting in the state-space formulation presented in [22].

$$\dot{X} = A_{SYS}.\Delta X + B.\Delta U \quad (3)$$

$$Y = C.\Delta X \quad (4)$$

Where

$$X = \left[\Delta E_q^{'} \quad \Delta\delta \quad \Delta\omega \quad \Delta E_{fd}\right] \quad (5)$$

$$\Delta u = [\Delta T_M \quad \Delta V_{ref}] \quad (6)$$

The matrices of Figure 1 are determined by applying Equations (3) and (4), while the corresponding state space representation of the test system, as given in Equation (5), is provided in [22].

For the open-loop test system, the system matrix associated with Equation (3) has a dimension of 4×4.

$$A_{SYS} = \begin{bmatrix} -0.4304 & -0.1654 & 0 & 0.1695 \\ 0 & 0 & 314 & 0 \\ -0.1000 & -0.2000 & 0 & 0 \\ 0 & -76.9468 & 0 & -5 \end{bmatrix}$$

Matrix 'B', as expressed in Equation (3), possesses a 4×2-dimensional configuration.

$$B = \begin{bmatrix} 0 & 0 \\ 0 & 0 \\ 0.2110 & 0 \\ 0 & 2000 \end{bmatrix}$$

Matrix 'C', as expressed in Equation (4), exhibits a 1×4-dimensional configuration.

$$C = [0 \quad 0 \quad 1 \quad 0]$$

By employing MATLAB, the open-loop transfer function derived for the test system, prior to the addition of any controller, is

$$\frac{0.2111s^3+1.146s^2+50.43s+1.091e-011}{s^4+5.43s^3+291.3s^2+276.8s+11910}$$

The system represented by Equation (5) consists of 4 state variables, which directly correspond to the fourth-order denominator of the derived transfer function. As a result, the system matrix A_{sys}yields 4 distinct eigenvalues that characterize the dynamic stability of the test system. The eigenvalues λ_i of the matrix are subsequently determined through the evaluation of its determinant.

$$det(A_{SYS} - \lambda I) = 0 \quad (\text{When } u = 0, \text{for all } t) \qquad (7)$$

$$\lambda_k = \sigma_k \pm i\omega_k \qquad (8)$$

In Equation (8), the real part, σ_k, represents the damping characteristic of the system, while the imaginary part, ω_k, corresponds to the oscillatory frequency of the response [19].

$$f_k = \omega_k/2\pi \qquad (9)$$

The Damping Ratio (DR), ζ_k is mathematically defined as stated in reference [19]

$$\zeta_k = \frac{-\sigma_k}{\sqrt{\sigma_k^2+\omega_k^2}} \qquad (10)$$

Table 1. Modal eigenvalues derived for the network

Mode #	Without control	DR (ζ)	Frequency (rad/sec)
$\Lambda_{1,2}$	-2.6863 ±15.4370 i	0.1730	15.6
$\Lambda_{3,4}$	-0.0243±7.1200 i	0.0034	7.76

In Table 1, Mode 2 exhibits a DR of 0.0034, which is notably smaller than that of Mode 1, making it a key factor in assessing the dynamic stability of the test system. Due to its significantly low damping value, this mode is designated as the critical mode. To effectively improve the DR associated with this critical mode, a PSS is introduced and applied to the test system.

3. PSS

In order to mitigate the adverse effects of negative damping, a PSS is installed within the generator, as illustrated in Figure 1. The PSS damping controller consists of three fundamental blocks. The first is a Gain block, which ensures adequate damping is applied to the critical oscillatory modes of the system. The second is a Washout block, which acts as a high pass filter, and it is obviated. The third block is a lead-lag constant $(\boldsymbol{T_1})$ and $(\boldsymbol{T_2})$ is to provide sufficient damping to the generator. The transfer function of PSS is given as

$$\boldsymbol{G(s) = K_{PSS}\frac{(1+sT_1)sT_W}{(1+sT_2)(1+sT_W)}} \qquad (11)$$

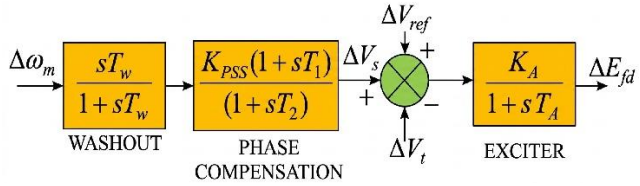

Fig. 2 PSS damping controller

The PSS receives the speed deviation signal, i.e.$\Delta\omega_m$, representing the difference between the actual rotor speed and the synchronous reference speed, as its input. The corresponding output generated by the damping controller is expressed in the form of a voltage deviation signal, i.e., ΔV_S This output is then introduced at the summation junction, where it is algebraically combined with the reference voltage $\Delta V_{ref}$and the terminal voltage ΔV_t feedback signal. The primary purpose of this integration is to suppress LFOs and to significantly improve the overall dynamic stability of the network. The system matrix (A_{SYS}) B and C equations corresponding to the PSS-integrated system are computed and presented as outlined in [22].

The equations after inclusion of PSS for Equations (3) and (4) are presented in [22]. The order system matrix of Equation (3) is increased to 5×5 from 4×4 due to the addition of a state variable (ΔV_S). As a result, the eigenvalues are increased from 4 to 5.

Table 2. Test system with PSS

Mode #	With PSS	DR (ζ)	Frequency (rad/sec)
$\Lambda_{1,2}$	-2.2235 ± 15.47i	0.1824	15.6
$\Lambda_{3,4}$	-0.3798±7.756i	0.0502	7.57
$\Lambda_{5,6}$	-10.4290	1	10.40

The eigenvalues obtained for the test system upon the incorporation of the PSS are presented and summarized in Table 2. A total of 5 modes are present. The eigenvalues corresponding to these modes are stable, and the DR of the critical mode $\Lambda_{3,4}$ is enhanced to 0.0501 from 0.0034. To

enhance the damping further by placing a TCSC on the transmission line.

4. TCSC

Figure 3 illustrates the configuration of the TCSC integrated with the test system depicted in Figure 1. For improving the stability of the system, TCSC is placed in series with the line and is modeled by means of an equivalent reactance X_{TCSC}. By varying the thyristor firing angle (α), the value of X_{TCSC}will vary, resulting in the reactance of the transmission line being varied [6].

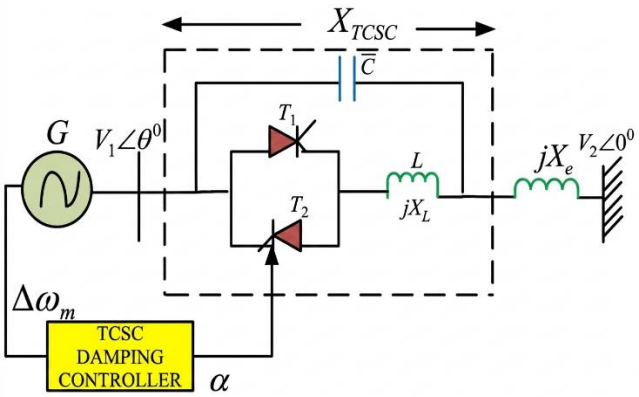

Fig. 3 Test system with TCSC

After incorporating TCSC in Figure 1, the state equations derived from Equations (3) are expressed as

$$\dot{\omega}_m = -\frac{K_2}{2H}\Delta E_q' - \frac{K_1}{2H}\Delta\delta + \frac{K_\alpha}{2H}\Delta\alpha - \frac{D\omega_s}{2H}\Delta\omega_m + \frac{1}{2H}\Delta T_m \quad (12)$$

$$E_{fd} = -\frac{1}{T_A}\Delta E_{fd} - \frac{K_A K_5}{T_A}\Delta\delta - \frac{K_A K_6}{T_A}\Delta E_q' + \frac{K_A}{T_A}\Delta V_{REF} \quad (13)$$

$$\Delta X_{TCSC} = -\frac{1}{T_{TCSC}}\Delta\alpha - \frac{1}{T_{TCSC}}\Delta X_{TCSC} \quad (14)$$

Figure 4 presents the transfer function of the TCSC damping controller. These blocks in TCSC are analogous to PSS in Figure 2. The input to Figure 4 is $\omega_m(=\Delta\omega/\omega_s)$, and the output is the thyristor conduction angle ($\Delta\sigma$). The reactance of the line in Figure 1 is regulated by varying the firing angle of thyristors. The desired value of compensation is obtained by varying the thyristor's conduction angle ($\Delta\sigma$). At steady-state conditions ($\Delta\sigma = 0$) , the net reactance of the line is $X_{EFF} = X_e - X_{TCSC}(\alpha_0)$. Whereas in a system that undergoes dynamic disturbances, the reactance of the line is modified to $X_{EFF} = X_e - X_{TCSC}(\alpha)$ [22]. Due to the presence of TCSC in the network, two additional state variables ($\Delta\alpha$), and (ΔX_{TCSC}) will be added to the Equation (3). As a result of this addition, the eigenvalues are increased from 4 to 6. In [22], all the data related to TCSC are provided for reference.

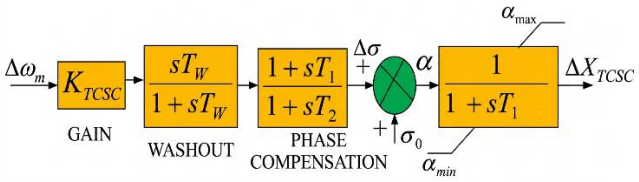

Fig. 4 TCSC damping controller

$E = 1.2235 + 0.8418i = 1.4851\angle 0.6026$
$\delta = 0.6029 \times \frac{180}{3.14} = 34.5439$
$T_M = 0.2784$; $V_{ref} = 1.1757$
$I_{dq} = 0.2161 + 0.1874i$; $I_d = 0.2161$;
$I_q = 0.1874$; $V_{dq} = 0.3086 + 1.1306i$;
$V_d = 0.3086$; $V_q = 1.1306$; $E_d' = 0.0012$;
$E_q' = 1.1836$; $E_{fd} = 1.4981$.

Adding the TCSC state variables to the Equation (5), becomes

$$X = \begin{bmatrix} E_q' & \Delta\delta & \Delta\omega & \Delta E_{fd} & \Delta\alpha & \Delta X_{TCSC} \end{bmatrix} \quad (15)$$

In [22], an equation for the TCSC system matrix is presented. To the Thyristor firing angle 145, the system matrix A_{TCSC} becomes

$$A_{TCSC} = \begin{bmatrix} -0.300 & -0.1 & 0 & 0.2 & 0 & 0 \\ 0 & 0 & 314 & 0 & 0 & 0 \\ -0.1 & -0.1 & 0 & 0 & 0.5 & 0 \\ -1646.3 & -74.7 & 0 & -5.0 & 2000 & 0 \\ 1.500 & 2.5 & -40 & 0 & -20.8 & 0 \\ 0 & 0 & 0 & 0 & 0 & 0.001 \end{bmatrix}$$

$$B_{TCSC} = \begin{bmatrix} 0 & 0 \\ 0 & 0 \\ 0.20 & 0 \\ 0 & 2000 \\ -4.20 & 0 \\ 0 & 0.001 \end{bmatrix}$$

$$C_{TCSC} = [0 \quad 0 \quad 1 \quad 0 \quad 0 \quad 0]$$

The transfer function after placing the TCSC becomes

$$\frac{0.211s^5+3.24s^4+70.55s^3+549.9s^2+23.68s+5}{s^6+26.18s^5+453.5s^4+6079s^3+17990s^2+10862s+4378}$$

Since the system matrix is of order 6, the resulting characteristic polynomial yields a denominator of the same order, giving rise to a total of six eigenvalues. Table 3 presents the eigenvalue analysis of the test system, illustrating all six eigenvalues obtained following the incorporation of the TCSC. A comparative analysis of Table 3 reveals that the DR of all eigenvalues is significantly enhanced when the TCSC controller is employed, relative to the case where only the PSS is utilized. The critical oscillatory mode undergoes a notable

shift further into the left-half of the complex plane, moving from its original position to a more stable location. Consequently, the damping ratio associated with the critical mode exhibits a substantial improvement, rising from 0.0034 to 0.195, which confirms the superior damping capability of the TCSC controller in suppressing low-frequency power system oscillations.

Table 3. Eigenvalues of the test system with TCSC

Mode #	With TCSC	DR (ζ)	Frequency (rad/sec)
$\Lambda_{1,2}$	-3.32 ± 17.10i	0.1910	17.4
$\Lambda_{3,4}$	-0.9510±4.79i	0.195	4.88
$\Lambda_{5,6}$	-0.042, -18	1,1	0.042,18

7. ROOBC

The ROOBC was formulated and implemented in [23] for the purpose of small-signal stability analysis in EPS. The Luenberger state observer is a well-established estimation technique that is conventionally applied to linear dynamical systems. The fundamental objective of this observer is to approximate the internal states of the system within a closed-loop structure in which state feedback control is utilized [24].

Considering the system equations presented in Equations (3) and (4), the output equation given in Equation (4) is assumed to satisfy the observability condition. The structural representation of the Luenberger observer is depicted in Figure 5.

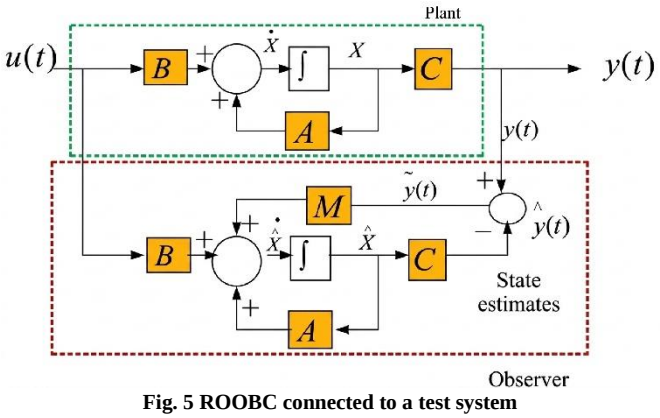

Fig. 5 ROOBC connected to a test system

Throughout the subsequent discussion, the symbol "Λ" is adopted to denote the estimated observer states, while the symbol "~" is utilized to represent the error between the original system states and their corresponding estimated states within the observer. The observer dynamics are simultaneously driven by both the input signal and the output signal of the original system. The measured output from the Equation (4) is continuously compared with its estimated counterpart ŷ, and the resulting discrepancy is employed as a corrective feedback term to improve state estimation accuracy. This error signal is subsequently multiplied by a real constant gain matrix M, and the resulting corrected signal is then injected into the integrator inputs of the observer to update and refine the state estimates continuously. The observer dynamic system is represented as

$$\dot{\hat{x}} = A\hat{x}(t) + Bu(t) + M\tilde{y}(t) \tag{16}$$

The dynamic behavior of the state estimation error vector, arising from the integration of the observer with the closed-loop control system, can be mathematically characterized as follows:

$$\tilde{x}(t) = x(t) - \hat{x}(t) \tag{17}$$

For Equation (17), differentiate on both sides, and it will become

$$\dot{\tilde{x}}(t) = \dot{x}(t) - \dot{\hat{x}}(t) \tag{18}$$

In Equation (18), substitute Equations (1) and (16), the resulting expression can be derived as

$$\begin{aligned}\dot{\tilde{x}}(t) &= Ax + bu - A\tilde{x} - Bu - MC(x - \hat{x}) \\ &= A(x - \hat{x}) - MC(x - \hat{x}) \\ &= (A - MC)\tilde{x}\end{aligned} \tag{19}$$

Taking the integral of Equation (19) yields the error in the state vector as:

$$\tilde{x} = \{e^{(A-MC)t}\}\tilde{x}(0) \tag{20}$$

This factor remains unaffected by the applied control input. The error $\tilde{x}$ will naturally diminish to zero over time. Provided that the matrix $'M'$ is appropriately configured to ensure that the error converges to zero, Equation (19) achieves asymptotic stability, meaning that all eigenvalues of the matrix $(A - MC)$ are located in the left half of the s-plane. Therefore, provided that the system represented by Equation (19) satisfies the observability condition, its states can be reconstructed using an n-dimensional observer structured in the following form.

$$\dot{\hat{x}} = (A - MC)\hat{x} + Bu + My \tag{21}$$

The matrix Mcan be appropriately designed to position the eigenvalues of Equation (21) at any desired location. It is noted that as long as the eigenvalues of $(A - MC)$possess negative real parts, regardless of the initial conditions, the estimated state will converge asymptotically toward X. For the observer described by Equation (20), specifying an initial state is not a requirement. Irrespective of what the initial state happens to be, the estimated state will eventually converge to the true state over time.

8. Algorithm for the Design of ROOBC

The step-by-step procedure for developing the ROOC is presented as follows:

Step-1: In [22], system data were presented

Step-2: By applying Equations (3) through (4), the system parameters are transformed into their corresponding state space representation

$$x = \begin{bmatrix} x_1 \\ x_2 \end{bmatrix}, A = \begin{bmatrix} A_{11} & A_{12} \\ A_{21} & A_{22} \end{bmatrix}, B = \begin{bmatrix} B_1 \\ B_2 \end{bmatrix}$$

$$C = [C_1 \quad C_2] \tag{22}$$

In the formulation of the ROOBC, a set of $(n-r)$ states is considered measurable, where $'n'$ signifies the order of the system matrix (A) and $'r'$indicates the rank of the output matrix C. As a result, in this specific scenario, a total of 6 states are found to be measurable."

The matrix A_{sys} is partitioned into four sub-matrices. The dimensional configurations of the sub-matrices are as follows: the first A_{11} is of order $r \times r$, the second A_{12} is of order $r \times (n-r)$, the third A_{21} is of order $(n-r) \times r$, and the fourth $A_{22}$is of order $(n-r) \times (n-r)$. Here, n corresponds to the order of the system matrix A, and r is indicative of the rank of the output matrix C.

The rank of a matrix B is defined as m. Accordingly, the sub-matrix B_1carries an order of $r \times m$, while the sub-matrix B_2 holds an order of $(n-r) \times m$.

The rank of the output matrix $C$is r. Matrix C is further partitioned into two sub-matrices, C_1, and C_2 where C_1 has an order of $r \times r$ and C_2has an order of $r \times (n-r)$.

Step-3: Transforms the states into a state space as

$$\bar{x}(t) = \bar{A}.x(t) + \bar{B}.u(t) \tag{23}$$

$$\bar{y}(t) = \bar{c}.\bar{x}(t) \tag{24}$$

$$\bar{x} = \begin{bmatrix} \bar{x}_1 \\ \bar{x}_2 \end{bmatrix}, \bar{A} = \begin{bmatrix} \bar{A}_{11} & \bar{A}_{12} \\ \bar{A}_{21} & \bar{A}_{22} \end{bmatrix}, \bar{B} = \begin{bmatrix} \bar{B}_1 \\ \bar{B}_2 \end{bmatrix}, \bar{C} = [I_m \quad 0]$$

Step-4: Compute $\bar{A}, \bar{B}$ by utilizing the following equations

$$\bar{A}_{11} = [C_1.A_{11} + C_2.A_{21}]C_1^{-1}$$
$$\bar{A}_{12} = -\bar{A}_{11}.C_2 + [C_1.A_{12} + C_2.A_{22}]$$
$$\bar{A}_{21} = A_{21}C_1^{-1} \text{ and } \bar{A}_{22} = A_{22} - A_{21}.C_1^{-1}.C_2$$
$$\bar{B}_1 = C_1.B_1 + C_2.B_2 \tag{25}$$

Step-5: Assume Λ to be a positive definite matrix

Step-6: To minimize the performance index in the design of an optimal controller, as follows:

$$J = \frac{1}{2}\int_0^\infty (x^T(t).\pi.x(t) + U^T(t).\Lambda.U(t).dt) \tag{26}$$

The P matrix obtained by solving the matrix Riccati equation is:

$$A^T.P + P.A - P.B.\Lambda^{-1}.B^T.P + \pi = 0 \tag{27}$$

Solving the Riccati equation for the solution of P (positive definite matrix) as well as K_0(state feedback gain matrix).

Step-7: Compute the observer gain matrix $\bar{L}$ from K_0 where $\bar{L} = K_0^T$

$$K_0 = R^{-1}.B^T.P \tag{28}$$

Step-7: Compute observer system matrices $(\bar{M}, \bar{N}, \bar{P})$ where $\bar{M}, \bar{N}, \bar{P}$ are the functions of $\bar{A}, \bar{B}, \bar{C}$and $\bar{L}$

$$M = \bar{A}_{22} - \bar{L}.\bar{A}_{12}$$
$$\bar{N} = B_2 - \bar{L}.B_1$$
$$\bar{P} = \bar{A}_{21} + \bar{A}_{22}.\bar{L} - \bar{L}\bar{A}_{11} - \bar{L}.\bar{A}_{12}.\bar{L} \tag{29}$$

Step-8: Determine the optimal state feedback gain matrix (K) by employing the relevant matrices $(A = \bar{A}_{22}^T, B = \bar{A}_{12}^T, Q)$ in the LQR optimal regulator design, with appropriately chosen weighting matrices R.

Step-9:Generate and display the plots for the desired parameters.

9. Design of TCSC in EPS with desired eigenvalues using ROOBC

TCSC connected to the test system with ROOBC, the equations are represented as n=6, m=2 and r=1.

$$A_{11} = [-0.300]$$
$$A_{12} = [-0.10 \quad 0 \quad 0.20 \quad 0 \quad 0]$$
$$A_{21} = \begin{bmatrix} 0 \\ -0.100 \\ -1646.3 \\ 1.5 \\ 0.1 \end{bmatrix}$$
$$A_{22} = \begin{bmatrix} 0 & 314 & 0 & 0 & 0 \\ -0.1 & 0 & 0 & 0.5 & 0 \\ -74.7 & 0 & -5 & 2000 & 0 \\ 2.5 & -40 & 0 & -20.8 & 0 \\ 0 & 0 & 0.01 & 0 & 0 \end{bmatrix}$$

The rank of B is m. The order of B_1 is 1×2, and the order of B_2 is 5×2. B matrix portioned into $B_1$and B_2.

$$B_1 = [0 \quad 0]$$

$$B_2 = \begin{bmatrix} 0 & 0 \\ 0.20 & 0 \\ 0 & 2000 \\ -4.20 & 0 \\ 0 & 0 \end{bmatrix}$$

C is portioned into $C_1$and C_2. The order of $C_1$is 1×1 and $C_2$is 1×5.

$$C_1 = [0.2]$$

$$C_2 = [0 \quad 1 \quad 0 \quad 0 \quad 0]$$

The $\bar{A}_{11}$ can be calculated from the equation.

$$\bar{A}_{11} = [C_1.A_{11} + C_2.A_{21}]C_1^{-1}$$

$$\bar{A}_{11} = \begin{bmatrix} -3.0859 & 0.1107 \\ -0.0585 & -3.1920 \end{bmatrix}$$

The $\bar{A}_{12}$ can be calculated from the equation.

$$\bar{A}_{12} = -\bar{A}_{11}.C_2 + [C_1.A_{12} + C_2.A_{22}]$$

$$\bar{A}_{12} = [-0.1200 \quad 0.8000. \quad 0.400 \quad 0.5000 \quad 0]$$

$\bar{A}_{21}$Can be calculated from the equation.

$$\bar{A}_{21} = A_{21}C_1^{-1}$$

$$\bar{A}_{21} = \begin{bmatrix} 0 \\ -0.005 \\ -8.2315 \\ 0.075 \\ 0.05 \end{bmatrix}$$

$\bar{A}_{22}$can be calculated from the equation.

$$\bar{A}_{22} = A_{22} - A_{21}.C_1^{-1}.C_2$$

$$\bar{A}_{22} = \begin{bmatrix} 0 & 314 & 0 & 0 & 0 \\ -0.1 & 0.5 & 0 & 0.5 & 0 \\ -74.7 & 823.15 & -5 & 2000 & 0 \\ 2.5 & -47.5 & 0 & -20.80 & 0 \\ 0.01 & -0.5 & 0 & 0 & 0 \end{bmatrix}$$

$\bar{B}_1$can be calculated

$$\bar{B}_1 = C_1.B_1 + C_2.B_2$$

$$\bar{B}_1 = [0.220 \quad 0.01]$$

The determination of the optimal state feedback gain matrix $(K)$is accomplished by obtaining the solution to the matrix Riccati equation. where the system matrix $A = \bar{A}_{22}^T$ and input matrix $B = \bar{A}_{12}^T$ are substituted with their respective partitioned counterparts.

$$\bar{A}_{22}^T = \begin{bmatrix} 0 & -0.1 & -74.7 & 2.5 & 0.01 \\ 314 & 0.5 & 82315 & -47.5 & -0.5 \\ -0.1 & 0.1 & 818.20 & -0.80 & -0.1 \\ 0 & 0.5 & 2000 & -20.80 & 0.92 \\ 0.001 & 0.002 & 0.0003 & 0.008 & 0.256 \end{bmatrix}$$

$$\bar{A}_{12}^T = \begin{bmatrix} -7.59 \\ 823.95 \\ 81.93 \\ 200.52 \\ 0.0060 \end{bmatrix}$$

The positive definite matrices Q, Λ are formulated and constructed as follows.

$$Q = \begin{bmatrix} 5 & 0 & 0 & 0 & 0 \\ 0 & 5 & 0 & 0 & 0 \\ 0 & 0 & 5 & 0 & 0 \\ 0 & 0 & 0 & 5 & 0 \\ 0 & 0 & 0 & 0 & 5 \end{bmatrix}$$

$$\Lambda = \begin{bmatrix} 3 & 0 & 0 & 0 \\ 0 & 3 & 0 & 0 \\ 0 & 0 & 3 & 0 \\ 0 & 0 & 0 & 3 \end{bmatrix}$$

Through the solution of the Matrix Riccati Equation, the matrix P is derived. This resulting Pmatrix is subsequently utilized to compute the state feedback gain matrix (K_0), which in turn serves as the basis for determining the observer gain matrix $(\bar{L})$.

$$P = \begin{bmatrix} 796.50 & 2.0821 & -139.143 & 78.7686 & 126.2289 \\ 2.08210 & 0.3784 & -1.3517 & -0.9066 & -0.3597 \\ -139.14 & -1.3517 & 32.9434 & -12.961 & -27.266 \\ 78.7686 & -0.9066 & -12.9610 & 12.0205 & 17.3148 \\ 26.23 & -0.3597 & -27.2665 & 17.3148 & 19418 \end{bmatrix}$$

$$K_0 = \Lambda^{-1}.B^T.P$$

$$K_0 = [21.1045 \quad 1.143 \quad 14.15 \quad 1.2057 \quad -1.6418]$$

The observer gain matrix $(\bar{L})$ can be obtained as

$$\bar{L} = K_0^T$$

$$\bar{L} = \begin{bmatrix} 21.1045 \\ 1.1431 \\ 14.1508 \\ 1.2057 \\ -1.6418 \end{bmatrix}$$

The system matrices $\bar{M}, \bar{N}, \bar{P}$ associated with the observer are evaluated by employing the following set of equations:

$$\bar{M} = \bar{A}_{22} - \bar{L}.\bar{A}_{12}$$

$$\bar{N} = B_2 - \bar{L}.B_1$$

$$\bar{P} = \bar{A}_{21} + \bar{A}_{22}\bar{L} - \bar{L}\bar{A}_{11} - \bar{L}.\bar{A}_{12}$$

$$\bar{M} = \begin{bmatrix} 160.1830 & -17076 & 1729 & 4232 & -0.1266 \\ 8.5763 & -941.374 & -93.611 & -228.71 & -0.0069 \\ 32.7044 & -3428 & -341.29 & -837.51 & -0.0849 \\ 11.6515 & 1041 & -99.5412 & -262.572 & -0.0072 \\ 12.4611 & 1352 & 134.4696 & 329.21 & 0.0099 \end{bmatrix}$$

$$\bar{N} = \begin{bmatrix} -4.2209 & -2.1104 \\ -0.0286 & -0.1143 \\ -2.8302 & 1998 \\ -4.4411 & -0..1206 \\ 0.5284 & 0.4642 \end{bmatrix}$$

$$\bar{P} = \begin{bmatrix} 17907 & 357 & 16017 & 13515 & 17746 \\ 949.82 & -0.7285 & 847.484 & 711.92 & 941 \\ 25357 & 13591 & 24091 & 22413 & 252 \\ 972 & -29.729 & 864 & 721 & 963 \\ 1366 & -0.7791 & -1219 & -1024 & -1353 \end{bmatrix}$$

$$R = 3$$

The optimal controller gain matrix (K) is determined and expressed as $\tilde{L}$.

$$K = \begin{bmatrix} 21.0145 \\ 1.1431 \\ 14.1508 \\ 1.2057 \\ -1.6418 \end{bmatrix}$$

Table 4. Stability check by means of eigenvalues

Mode #	With ROOBC	DR (ζ)	Frequency (rad/sec)
$\Lambda_{1,2}$	-3.95±19.32i	0.200	19.7
$\Lambda_{3,4}$	-0.7640 ±2.73i	0.2690	2.83
$\Lambda_{5,6}$	-0.046, -18.90	1.0,1.0	0.046,18.90

When the ROOBC is implemented alongside TCSC as a feedback controller, the critical eigenvalue undergoes a significant shift from 0.9510 ± 4.79i (Table 3) to -0.7640 ± 2.73i (Table 4). This transition leads to a considerable improvement in system damping, thereby resulting in enhanced overall system stability. Furthermore, an analysis of the dynamic response curves reveals that the ROOBC delivers superior stabilization performance in comparison to both the TCSC and PSS controllers.

10. Time Response Analysis

To evaluate the performance of the test system, a small disturbance equivalent to 1% of the mechanical input power ΔT_M is introduced at the generator. The operating conditions of the test system are established at $P = 1.0\,p.u$, $Q = 0.67\,p.u$, and $V_t = 1.0\,p.u$ [22].

The simulation results for the network are obtained using MATLAB software. Figure 6 illustrates the comparative time response analysis of the test system, depicting the rotor angle deviation *'Δδ'* of the generator under various control schemes.

The responses correspond to the system operating without any controller (represented by a black line with circles), with PSS (represented by a blue line), with TCSC (represented by a red line), and with ROOBC (represented by a pink line).

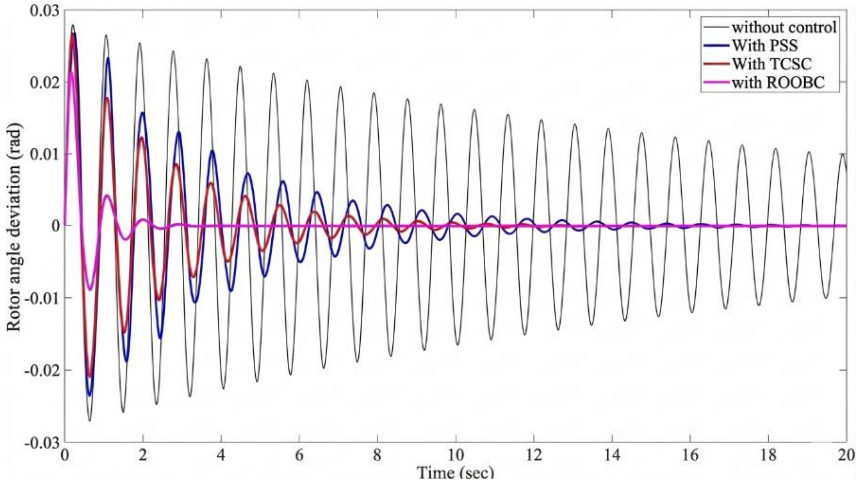

Fig. 6 Time response analysis of the test system

As illustrated in Figure 6, the damping performance of the system under different control configurations reveals the effectiveness. The settling time recorded for each scenario stands at 123.2857 s, 10.85 s, 4.23 s, and 2.37 s, while the corresponding peak overshoot values are 1.0095%, 0.8523%, 0.4261%, and 0.2786% for the uncontrolled system, PSS-based control, TCSC-based control, and the proposed ROOBC integrated with TCSC, respectively. A comparative analysis of

these figures confirms that the ROOBC–TCSC combination achieves the fastest attenuation of LFOs, outperforming standalone TCSC, conventional PSS, and the uncontrolled baseline. These analyses validate the superior damping capability of the proposed ROOBC with the TCSC framework in effectively suppressing LFOs across the EPS.

An analysis of Figure 6 reveals that the system equipped with ROOBC demonstrates the most favorable dynamic response characteristics, exhibiting the lowest amplitude deviations, the shortest settling time, minimal overshoot and undershoot, and the fastest recovery to its pre-disturbance steady-state condition compared to all other control configurations examined.

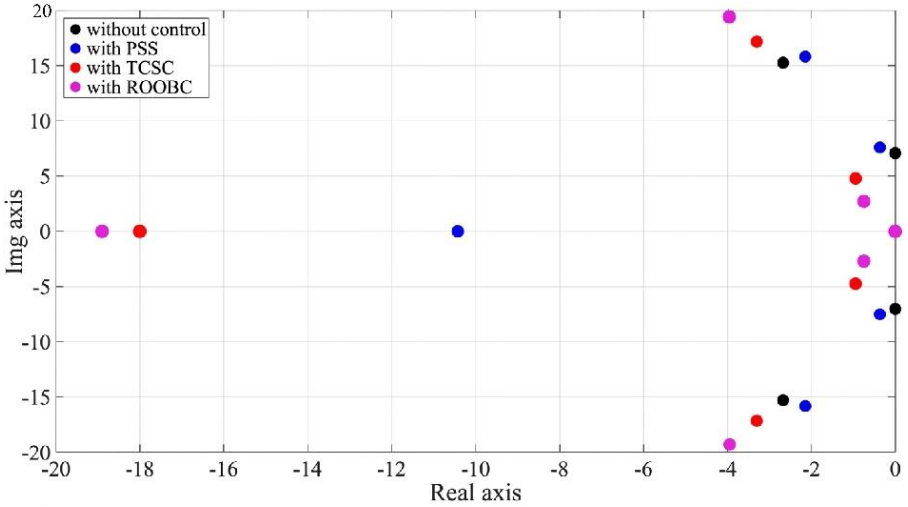

Fig. 7 Eigenvalues of the test system

Figure 7 depicts the eigenvalue distribution of the network under different control strategies. It is evident that the eigenvalues experience a greater shift toward the left half of the s-plane when TCSC is combined with ROOBC, in comparison to the other control approaches. This leftward migration of eigenvalues further confirms the improvement in the dynamic stability of the system achieved through the implementation of ROOBC. The key benefit of the ROOBC lies in its ability to effectively dampen oscillations while simultaneously reducing both the peak overshoot and settling time. However, the implementation of ROOBC becomes increasingly challenging in higher-order systems, primarily due to the difficulties associated with the measurement of system states and the fact that system nonlinearities are not taken into account. The issue of unavailable system variables can be addressed through alternative control strategies such as sliding mode controllers, observer-based sliding mode controllers, and fractional controllers.

11. Conclusion

This paper proposed an ROOBC integrated with TCSC to improve the dynamic stability of an SMIB system. The principal contributions of this work can be outlined as follows:

A mathematical model of the test system incorporating PSS, TCSC, and ROOBC has been developed to analyze LFOs. A structured methodology has been established to evaluate eigenvalues with PSS, TCSC, and ROOBC, demonstrating that the ROOBC shifts the eigenvalues further into the left half of the s-plane compared to other approaches. It has been demonstrated that the dynamic response of the test system is significantly improved when the ROOBC is applied at the nominal operating point. As a direction for future research, the current work can be extended by incorporating TCSC with a fractional order sliding mode observer-based optimal controller, further enhanced through the integration of ANN and fuzzy control strategies.

Conflicts of Interest

There is no known conflict of interest associated with the research work mentioned in the paper. The study in the paper was carried out independently. So it was not influenced by any personal, commercial, or financial aspects or relationships. There was no external organization involved at any role in the design of the proposed system. So, working, the results and conclusions presented in research work are solely based on academic and technical considerations. Hence, the publication does not involve any conflict of interest.

References

[1] Vijay Vittal et al., *Power System Control and Stability*, 3rd ed., John Wiley & Sons, 2019. [Google Scholar] [Publisher Link]

[2] A.E. Hammad, "Analysis of Power System Stability Enhancement by Static Var Compensators," *IEEE Transactions on Power Systems*, vol. 1, no. 4, pp. 222-227, 1986. [CrossRef] [Google Scholar] [Publisher Link]

[3] Narain G. Hingorani, and Laszlo Gyugyi, *Understanding FACTS, Concepts and Technology of Flexible AC Transmission System*, John Wiley & Sons, 1999. [Google Scholar] [Publisher Link]

[4] Juan M. Ramírez, and Isidro Castillo, "PSS and FDS Simultaneous Tuning," *Electric Power Systems Research*, vol. 68, no.1, pp. 33-40, 2004. [CrossRef] [Google Scholar] [Publisher Link]

[5] Q.J. Liu et al., "Adaptive Nonlinear Coordinated Excitation and STATCOM Controller based on Hamiltonian Structure for Multi-Machine Power System Stability Enhancement," *IEE Proceedings - Control Theory and Applications*, vol. 150, no. 3, pp. 285-294, 2003. [CrossRef] [Google Scholar] [Publisher Link]

[6] X. Lei, X. Li, D. Povh, "A Nonlinear Control for Coordinating TCSC and Generator Excitation to Enhance the Transient Stability of Long Transmission," *Electric Power Systems Research*, vol. 59, no. 2, pp. 103-109, 2001. [CrossRef] [Google Scholar] [Publisher Link]

[7] Li-Jun Cai, and I. Erlich, "Simultaneous Coordinated Tuning of PSS and FACTS Damping Controller in a Large Power System," *IEEE Transactions on Power Systems*, vol. 20, no. 1, pp. 294-300, 2005. [CrossRef] [Google Scholar] [Publisher Link]

[8] B. Kalyan Kumar, S.N. Singh and S.C. Srivastara, "Placement of FACTS Controllers Using Model Controllability Indices to Damp Out Power System Oscillations," *IET Generation, Transmission and Distribution*, vol. 1, no. 2, pp. 209-217, 2007. [CrossRef] [Google Scholar] [Publisher Link]

[9] Farshad Mogharrab Tehrani, Ghazanfar Shahgholian, and Hossein Pourghassem, "Dynamic Study and Stability Analyze of Damping Cohefision and Reactance in TCSC Controller Connected on Optimization SMIB System," *2011 IEEE 3rd International Conference on Communication Software and Networks*, Xi'an, China, pp. 270-274, 2011. [CrossRef] [Google Scholar] [Publisher Link]

[10] M. Noroozian, and G. Adersson, "Damping of Power System Oscillations by use of Controllable Components," *IEEE Transactions on Power Delivery*, vol. 9, no. 4, pp. 2046-2054, 1994. [CrossRef] [Google Scholar] [Publisher Link]

[11] X.R. Chen et al., "Controlled Series Compensation for Improving the Stability of Multi-Machine Power Systems," *IEE Proceedings Generations, Transmission and Distribution*, vol. 142, no. 4, pp. 361-366, 1995. [CrossRef] [Google Scholar] [Publisher Link]

[12] Jaewon Chang, and J.H. Chow, "Time-Optimal Series Capacitor Control for Damping Inter-Area Modes in Interconnected Power Systems," *IEEE Transactions on Power Systems*, vol. 12, no. 1, pp. 215-221, 1997. [CrossRef] [Google Scholar] [Publisher Link]

[13] Juan Miguel Gonzalez, Claudio A. Canizares, and Juan M. Ramirez, "Stability Modeling and Comparative Study of Series Vectorial Compensators," *IEEE Transactions on Power Delivery* , vol. 25, no. 2, pp. 1093-1103, 2009. [CrossRef] [Google Scholar] [Publisher Link]

[14] A. Ghosh et al., "Power System Stabilizer based on Adaptive Control Techniques," *IEEE Transactions on Power Apparatus and Systems*, vol. PAS-103, no. 8, pp. 1983-1989, 1984. [CrossRef] [Google Scholar] [Publisher Link]

[15] H. Shayeghi, H.A. Shayanfar, and A. Jalli, "Load Frequency Control Strategies: A State-of-the-Art Survey for the Researcher," *Energy Conversion and Management*, vol. 50, no. 2, pp. 344-353, 2009. [CrossRef] [Google Scholar] [Publisher Link]

[16] George Ellis., *Observers in Control Systems: A Practical Guide*, 1st ed., Academic Press, 2002. [CrossRef] [Google Scholar] [Publisher Link]

[17] Arash Golabi, Mohammad Taghi Hamidi Beheshti, and Mohammad Hasan Asemani, "Dynamic Observer-based Controllers for Linear Uncertain Systems," *Journal of Control Theory and Applications*, vol. 11, no. 2, pp. 193-199, 2013. [CrossRef] [Google Scholar] [Publisher Link]

[18] Mania Pavella, "Power System Stability and Control Comparative Analysis," *IFAC Proceedings Volumes*, vol. 30, no. 6, pp. 63-75, 1997. [CrossRef] [Google Scholar] [Publisher Link]

[19] Bernard Friedland, *Control System Design: An Introduction to State-Space Methods*, Dover Publications, 2005. [Google Scholar] [Publisher Link]

[20] Kemin Zhou, and John C. Doyle, *Essentials of Robust Control*, Prentice Hall, 1998. [CrossRef] [Google Scholar] [Publisher Link]

[21] Guangzeng Yu et al., "Coordination of PSS and FACTS Damping Controllers to Improve Small Signal Stability of Large-Scale Power Systems," *CSEE Journal of Power and Energy Systems*, vol. 5, no. 4, pp. 507-514, 2019. [CrossRef] [Google Scholar] [Publisher Link]

[22] Debasish Mondal, Abhijit Chakrabarti and Aparajita Sengupta, *Power System Small Signal Stability and Control*, Academic press, 2014. [CrossRef] [Google Scholar] [Publisher Link]

[23] N. Abu-Tabak, J.Y. Auloge, and P. Auriol, "Reduced-Order Observer Design for Small-Signal Multi-Machine Power System Stability Improvement by Optimal Control," *2008 Second UKSIM European Symposium on Computer Modeling and Simulation*, Liverpool, UK, pp. 370-375, 2008. [CrossRef] [Google Scholar] [Publisher Link]

[24] Cong-Ran Zhao, and Xue-Jun Xiehao, "Output Feedback Stabilization Using Small-Gain Method and Reduced-Order Observer for Stochastic Nonlinear Systems," *IEEE Transactions on Automatic Control*, vol. 58, no. 2, pp. 523-529, 2012. [CrossRef] [Google Scholar] [Publisher Link]